RESEARCH ARTICLE

Identification of potential SARS-CoV-2 Nsp1 inhibitors from *Piper sarmentosum* Roxb. using molecular docking

Saw, K.C.[1], Ahmad Mokhtar, A.M.[1], Ismail, N.I.[2*]

[1]School of Technology Industry, Universiti Sains Malaysia, 11800 USM, Penang, Malaysia
[2]School of Biological Sciences, Universiti Sains Malaysia, 11800 USM, Penang, Malaysia
*Corresponding author: nurul.ismail@usm.my

ABSTRACT

Nsp1 in SARS-CoV-2 is a key protein that increases the virus's pathogenicity and virulence by binding to the host ribosome and blocks the 40S ribosomal subunit channel, which effectively impedes the mRNA translation as well as crippling the host immune system. Previous studies revealed that the N-terminal in Nsp1 is part and parcel of Nsp1 efficiency, and mutations in its core residues have weakened the protein's. This knowledge persuades us to carry out the *in silico* screening on plant compounds of *Piper sarmentosum* Roxb. against the five target residues which are Glu36, Glu37, Arg99, Arg124 and Lys125. Potential compounds were tested for their druggability. As a result, we identified five out of 112 compounds including stigmasterol, N-feruloyltyramine, beta-Sitosterol, 13-(1,3-benzodioxol-5-yl)-*N*-(2methylpropyl) trideca-2,4,12-trienamide and *N*-(2-methylpropyl) octadeca-2-4dienamide in *Piper sarmentosum* Roxb. as potential inhibitors for Nsp1. These compounds formed at least a hydrophobic, hydrogen bonding or π-cation interactions with the protein. Furthermore, SwissADME analysis and the number of bindings to the target residues suggest that N-feruloyltyramine is the ideal inhibitor candidate against SARS-CoV-2 at its N-terminal of Nsp1. Lastly, the interaction with N-feruloyltyramine increased flexibility in the loop regions of N-terminal Nsp1, especially residues 54 to 70, with residue 59 showing the highest fluctuation, potentially affecting the protein's stability and function due to the correlation between RMSF and protein function.

Keywords: Computational biology; N-feruloyltyramine; Nsp1; *Piper sarmentosum* Roxb.; SARS-CoV-2.

INTRODUCTION

The non-structural protein (Nsp) is crucial for SARS-CoV-2 replication and transcription especially to assemble new virions, with the aid of structural protein (Arya *et al*., 2021). Nsp1 is a major virulence factor that contributes to the efficient replication of the virus (Semper *et al*., 2021). This protein binds with the 40S ribosomal subunit and host mRNA's endonucleolytic cleavage that downregulates host protein translation (Kamitani *et al*., 2009; Gorkhali *et al*., 2021). This lowers the expression level of several host factors that signal the presence of viral infection and subsequently, cause slow or no response from the innate immune system (Arya *et al*., 2021). The protein also enables the virus to break through the host immune response by suppressing type 1 interferon expression in the infected cells (Narayanan *et al*., 2008; Gorkhali *et al*., 2021).

The protein is a 180 amino acid (aa) long protein which has a flexible N-terminal domain (aa 1-128) and C-terminal domain (aa 148-180), and a small linker region that connects those two domains (aa 129-147) (Schubert *et al*., 2020; Yuan *et al*., 2021; Graziadei *et al*., 2022). Three-dimensional model of a full-length SARS-CoV-2 Nsp1 via nuclear magnetic resonance (NMR) analysis or crystallization revealed the structure that consist of an antiparallel β-barrel capped by an α-helix, two parallel 3$_{10}$ helices, and an additional β strand constitute its main structure as shown in Figure 1 (Almeida *et al*., 2007; Clark *et al*., 2021; Semper *et al*., 2021).
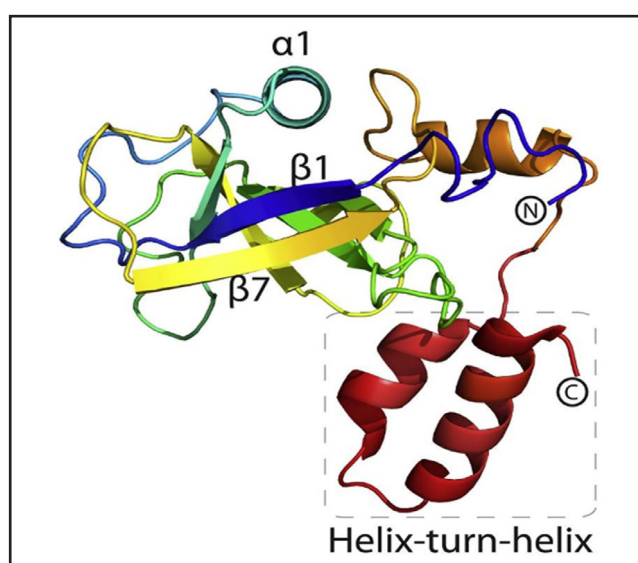
Figure 1. Structural characterization of SARS-CoV-2 Nsp1. A complete structure that runs from the N-terminus (highlighted in blue), an α1 (highlighted in turquoise), a β7 (highlighted in yellow), and the C-terminus (highlighted in red). Adapted from Semper *et al*. (2021), Figure 4.

Although the C-terminal is crucial part in Nsp1, whereby it positions itself at the 40S mRNA entry channel and hence, blocks the host mRNA translation, the C-terminal is highly flexible and only gains its distinctive structural helicity when it interacts with the 40S and 80S ribosome via electrostatic and hydrophobic interactions (Kamitani *et al.*, 2009; Schubert *et al.*, 2020; Thoms *et al.*, 2020; Yuan *et al.*, 2020). Therefore, it cannot be crystallized in either full-length or isolation (Clark *et al.*, 2021; Kumar *et al.*, 2021; Semper *et al.*, 2021). Therefore, the C-terminal is not an ideal target protein to undergo molecular docking, which brings in the current focus on the N-terminal instead.

Unlike the C-terminal, the SARS-CoV-2 Nsp1 N-terminal structure was successfully crystallized with PDB ID: 7K3N (aa 13-127) and PDB ID: 7K7P (aa 10-127) (Clark *et al.*, 2021; Semper *et al.*, 2021). However, the globular N-terminal did not directly obstruct the 40S mRNA channel to suppress the host mRNA translation (Banerjee *et al.*, 2020; Shi *et al.*, 2020). It interacts with the 5' UTR or the leader sequence of the viral RNA (vRNA), prevents the inhibition of the Nsp1-C-terminal-40S ribosome complex, and facilitates the precise translation of vRNA (Banerjee *et al.*, 2020; Shi *et al.*, 2020). Moreover, the N-terminal and its domains/residues contribute to increasing the Nsp1's efficiency in inducing mRNA translational shutoff and decay by destabilizing the functions of mRNA, stabilizing the interaction between Nsp1 and host ribosome and mRNA, as well as safeguarding the viral transcripts from the virus very own cleavage activity (Mendez *et al.*, 2021).

Mendez *et al.* (2021) showed the importance of each residue in the N-terminal, central domain, and C-terminal by mutating certain charged, conserved, and surface exposed residues. They figured that mutants Arg99 and Arg124/Lys125 have profound negative effects on Nsp1's function. Mutations at these residues could prevent the formation of the Nsp1 ribosome complex, destabilize the binding between Nsp1's C-terminal and 40S ribosomal unit, suppress the translation of the viral transcripts, and even possibly "lock up" Nsp1 in a translationally inhibited state (Mendez *et al.*, 2021). Meanwhile, mutants Glu36/Glu37 have a lesser negative effect on Nsp1's ribosomal binding and inhibition of mRNA translation (Mendez *et al.*, 2021). Thus, residues Glu36, Glu37, Arg99, Arg124, and Lys125 are the residues targeted for docking of the plant compounds.

Piper sarmentosum Roxb. commonly known as 'kaduk' or 'daun kaduk' in Malay, is a terrestrial plant native in Malaysia (Figure 2) (Samy *et al.*, 2014). This plant also can be found in many Asia countries such as Thailand, Indonesia, India, and China (Sun *et al.*, 2020). This creeping terrestrial plant has smooth dark green and ubiquitous heart-shaped leaves. It is often used in cooking and as traditional medicine (Rukachaisirikul *et al.*, 2004). *Piper sarmentosum* Roxb. is reported to have antibacterial, antiprotozoal, antimalarial, antioxidant, hypoglycaemic and antiviral effects (Hamidi *et al.*, 1996; Zaidan *et al.*, 2005; Sun *et al.*, 2020). To the best of our knowledge, there is no study on *Piper sarmentosum* Roxb. and its extracts as potential SARS-CoV-2 inhibitors yet.

MATERIALS AND METHODS

Multiple Sequence Alignment of Wild-type N-terminal Nsp1 SARS-CoV-2 and its Omicron Subvariant

Alterations were made to the amino acid sequence of the wild-type N-terminal Nsp1 SARS-CoV-2 (125aa) such as substituting a single amino acid for BA.1 at R99C, BA.2 and BA.3 at P62T, and deleting five amino acids (GHVMV) from position 82 for BA.4 (Singh *et al.*, 2022; Ak, 2023; Savellini *et al.*, 2023). The protein FASTA sequences of the wild-type, BA.1, BA.2, BA.3 and BA.4 were submitted to MultAlin (http://multalin.toulouse.inra.fr/multalin/) for multiple sequences alignment (Corpet, 1988).

Structural Comparison of N-terminal Nsp1 of SARS-CoV-2 between Wild-type and BA.1, BA.2, BA.3 and BA.4
The altered N-terminal Nsp1 of SARS-CoV-2 protein sequences for BA.1, BA.2, BA.3 and BA.4 were sent for protein modelling using SWISS-MODEL. Each of the modelled protein structures was superimposed with the wild-type N-terminal Nsp1 structure in PyMOL and the generated root mean square deviation (RMSD) results were recorded.

Structural Stability Prediction of N-terminal Nsp1 of SARS-CoV-2 among BA.1, BA.2 and BA.3
The PDB file of the wild-type N-terminal Nsp1 of SARS-CoV-2 was uploaded into DynaMut2 server (https://biosig.lab.uq.edu.au/dynamut2) in the single mutation category (Rodrigues *et al.*, 2021). The single amino acid substitution information was provided in the 'mutation details' section based on BA.1, BA.2 and BA.3. Data from the predicted protein stability due to amino acid substitution in these three Omicron subvariants were recorded.

Molecular Docking

Protein Structure Preparation
The PDB 3D protein structures of SARS-CoV-2 Nsp1 (N-terminal), 7K3N and 7K7P had shortened protein sequences of just reaching 116 aa and 117 aa in length, respectively. The structures were visualized using PyMOL version 2.5.0 (https://www.pymol.org/pymol.html) and AutoDock Tools. This means they had missing residues including the target residues of Arg124 and Lys125. Therefore, the FASTA sequence of SARS-CoV-2 Nsp1 with NCBI sequence reference of YP_009725297.1 was submitted for molecular modelling in SWISSMODEL (https://swissmodel.expasy.org/) (Singh *et al.*, 2021). The best model that represented the N-terminal and contained all the target residues were downloaded in PDB format. Then, the protein structure was optimised using AutoDock Tools (Trott & Olson, 2010; Eberhardt *et al.*, 2021). The optimization steps involved the removal of water molecules and the addition of polar hydrogen as well as Kollman charges (Trott & Olson, 2010; Adejoro *et al.*, 2020; Eberhardt *et al.*, 2021). The final step of protein preparation was saving the prepared/optimized structure

Figure 2. Picture of the pointed pepper or *Piper sarmentosum* Roxb. taken at a riverbank at Jalan Gangsa, Greenlane Heights, 11600 Jelutong, Penang (latitude: 5.392001778259563, longitude: 100.29819142495589).

of N-terminal in PDBQT file format (Trott & Olson, 2010; Eberhardt *et al.*, 2021).

Ligand Structures Preparation
A total of 112 natural plant compounds of *Piper sarmentosum* Roxb. were retrieved from PubChem (https://pubchem.ncbi.nlm. nih.gov/taxonomy/405319) in SDF format (Adejoro *et al.*, 2020). Afterward, all the 112 SDF files were converted into PDB format by using OpenBabel version 3.1.1 (https://github.com/openbabel/ openbabel/releases/tag/openbabel-3-1-1) (Trott & Olson, 2010; O'Boyle *et al.*, 2011; Eberhardt *et al.*, 2021). Each of the plant compounds in the PDB file format underwent ligand preparation in AutoDock Tools version 1.5.7 (https://ccsb.scripps.edu/mgltools/ downloads/) before converting them into PDBQT file format (Sanner, 1999; Trott & Olson, 2010; Eberhardt *et al.*, 2021).

Determination of Docking Site
The grid box is prepared to cover the target residues Glu36, Glu37, Arg99, Arg124, and Lys125 with sufficient space for the ligands to dock (Trott & Olson, 2010; Eberhardt *et al.*, 2021). The grid box was set according to these values: (centre = 10.693, centre_y = 13.136, centre_z = 47.254) and (size_x = 90, size_y = 92, size_z = 102). This parameter setting was saved as a grid.txt file (Trott & Olson, 2010; Eberhardt *et al.*, 2021).

Molecular Docking Simulation
A configuration file (config.txt) was generated based on parameters set in the grid.txt file (centre and size of x, y, and z). In addition, we set energy range = 4, the number of modes = 10, and exhaustiveness = 10 (Trott & Olson, 2010; Eberhardt *et al.*, 2021). AutoDock Vina version 1.2.3 (https://github.com/ccsb-scripps/AutoDock-Vina/ releases) was used to screen the 122 plant compounds against the N-terminal. However, to screen all 122 plant molecules in one run, Padre, the Perl IDE (https://padre.perlide.org/) was employed. The PerlScript file was retrieved from https://drive.google.com/file/d/1 fVBHorqXI0mwkb6BoOH4wc6ioiiF8R/view. Once the five necessary files had been prepared (protein.pdbqt, ligand.pdbqt, ligand.txt, config.txt, and Perl_script.txt), the docking process in AutoDock Vina was carried out.

Protein-Ligand Binding Analysis
The docked compounds were filtered out by determining which of them managed to interact with the five target residues to be considered potential compounds with the lowest binding affinity (kcal/mol). Each of the potential plant compounds of *Piper sarmentosum* Roxb. had their output logfiles (PDBQT) and the prepared protein file (protein.pdbqt) to be imported into PyMOL and were exported as a molecule in pdb format based on the best protein-ligand conformation. These pdb files were later subjected to protein-ligand conformation and molecular interactions analysis in Proteins*Plus* (https://proteins.plus/) and ProteinLigand Interaction Profiler (PLIP) (https://plip-tool.biotec.tu-dresden.de/plipweb/ plip/index) (Fährrolfes *et al.*, 2017; Schöning-Stierand *et al.*, 2020; Adasme *et al.*, 2021).

SwissADME Analysis
The successful ligands were analysed for their ADME, pharmacokinetics and drug-likeness properties in SwissADME (http://www.swissadme.ch/) based on their canonical simplified molecular input line entry system (SMILES) as the input (Daina *et al.*, 2017).

Molecular Dynamic (MD) Simulation
CABS-flex 2.0 (https://biocomp.chem.uw.edu.pl/CABSflex2) was used the carry out the MD simulation on the protein structure of wild-type N-terminal Nsp1 of SARS-CoV-2 and the ligand N-feruloyltyramine complex to investigate the best potential

inhibitor and the protein itself (Kuriata *et al.*, 2018). MD simulation explores the dynamic behaviour and interactions of these molecules at the atomic level, providing insights into their structural changes and binding mechanisms. Each of the two protein files was submitted for MD simulation analysis in CABS-flex 2.0 with default parameters, separately. The fluctuation plot data were downloaded once the simulation was completed and plotted for comparison between the N-terninal Nsp1 and its ligand-protein complex.

RESULTS

Out of the 112 compounds that we screened in Autodock Vina, five compounds which are stigmasterol, N-feruloyltyramine, beta-Sitosterol, 13-(1,3-benzodioxol-5-yl)-*N*-(2-methylpropyl) trideca-2,4,12-trienamide and *N*-(2methylpropyl) octadeca-2-4-dienamide were able to interact at least one of the target residues (Glu36, Glu37, Arg99, Arg124 and Lys125) with relatively good binding affinity. PLIP detected molecular interactions that exist between these five compounds and the N-terminal such as hydrophobic and π-cation interactions, and hydrogen bonding. We also analysed the five compounds using ADME, pharmacokinetic and SwissADME for drug-likeness analysis.

**SARS-CoV-2's Nsp1 N-Terminal Crystal Structure**
Based on the given SARS-CoV-2 leader protein/Nsp1 FASTA as the input, the SWISS-MODEL generated 12 templates and the best model of the SARS-CoV-2 Nsp1 crystal structure, 7K3N.1.A. Figure 3 illustrated 3D structure of Nsp1 N-terminal protein modelled by SWISS-MODEL.

Multiple Sequence Alignment of Nsp1's N-terminal of SARS-CoV-2 of Omicron subvariants
Several studies have reported on mutations that occurred in the N-terminal of Nsp1 of SARS-CoV-2 of Omicron subvariants. Single amino acid substitution was observed in subvariants BA.1 (R99C) and, BA.2 and BA.3 shared the same substitution at P62T (Singh *et al.*, 2022; Savellini *et al.*, 2023). Additionally, a five amino acid deletion starting at position 82, was seen in some subvariants of BA.4 (Ak, 2023). However, there are no studies that report on such mutations in BA.5 and BA.6. Therefore, the wild-type sequence
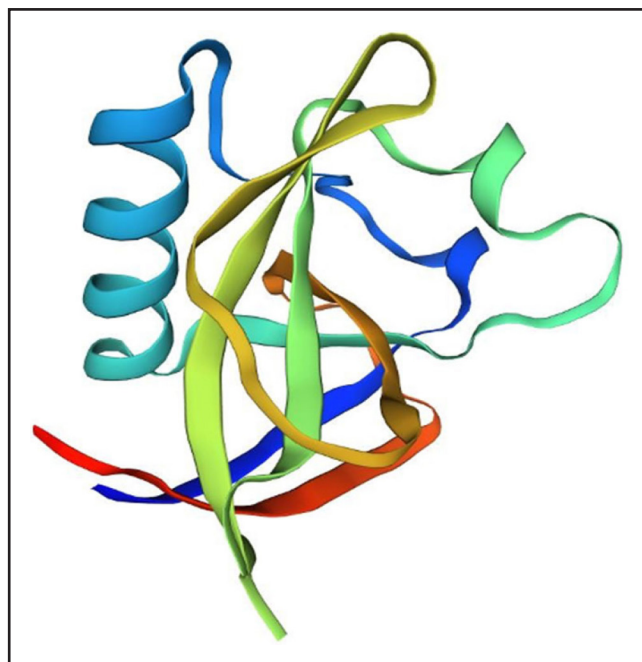
Figure 3. Crystal structure of N-terminal of SARS-CoV-2 Nsp1 protein modelled by SWISS-MODEL.
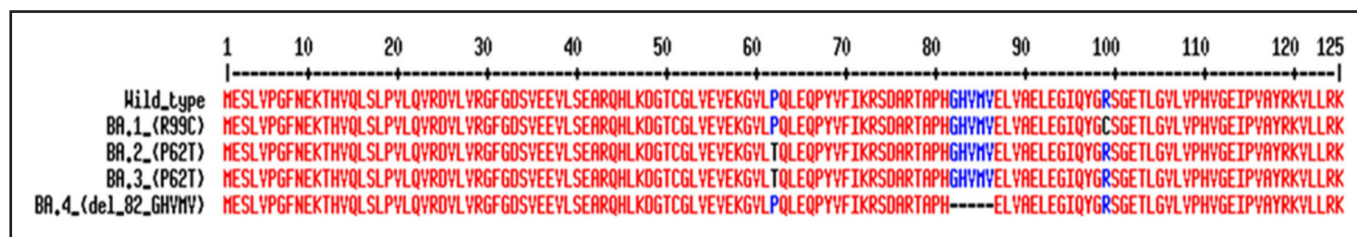
Figure 4. Multiple sequence alignment of N-terminal of Nsp1 of SARS-CoV-2 of wild-type and its Omicron subvariants: BA.1, BA.2, BA.3 and BA.4.

and the sequences of Omicron subvariants of BA.1, BA.2, BA.3 and BA.4 of Nsp1's N-terminal of SARS-CoV-2 were aligned using MultAlin (Figure 4).

RMSD Values of N-terminal of Nsp1 of Omicron Subvariants against Wild-type
The superimposition of Nsp1 N-terminal protein structure between wild-type and each of the Omicron subvariants (BA.1, BA.2, BA.3 and BA.4) yielded RMSD values of 0.219, 0.222, 0.222 and 0.224, respectively (Table 1).

N-terminal Nsp1 Protein Structure Stability Analysis
DynaMut2 was used to analyse the structural stability of the N-terminal of Nsp1 of BA.1, BA.2 and BA.3 which had single amino acid substitution (Table 2). This analysis cannot be carried out for BA.4 as there are no available tools/software, including DynaMut2, to analyse the stability effect resulted from deletion. The R99C in BA.1 was predicted to slightly stabilize the structure with positive Gibbs free energy of 0.02 kcal/mol. On the other hand, the P62T in both BA.2 and BA.3 were predicted to have destabilising effect on the N-terminal Nsp1 structure with negative Gibbs free energy of -0.35 kcal/mol.

Molecular Docking Output on Target Binding Residues
Virtual screening of the 112 active compounds of *Piper sarmentosum* Roxb. was conducted by using AutoDock Vina. Five compounds were able to interact with at least one of the target residues (Table 3). Stigmasterol had the lowest binding affinity (the most negative) which is -4.7 kcal/mol but interacted with only one target residue that is Arg99. On the other hand, N-feruloyltyramine interacted with three target residues that are Arg99, Arg124 and Lys125 with binding affinity -4.4 kcal/mol. This was followed by beta-sitosterol (Arg99), 13-(1,3-benzodioxol-5-yl)-N-(2-methylpropyl) trideca-2,4,12-trienamide (Glu36) and, N-(2-methylpropyl) octadeca-2-

Table 1. Omicron subvariants and their respective RMSD (Å) values following superimposition between their protein structures and wild-type of Nsp1 N-terminal

Omicron subvariants	RMSD (Å)
BA.1 (R99C)	0.219
BA.2 (P62T)	0.222
BA.3 (P62T)	0.222
BA.4 (del_82-GHVMV)	0.224

Table 2. Omicron subvariants and their protein structure stability due to single amino acid substitution

| Omicron Subvariants	Predicted Stability Change ($\Delta\Delta G^{Stability}$)	Remarks
BA.1 (R99C)	0.02 kcal/mol	Stabilizing
BA.2 (P62T)	-0.35 kcal/mol	Destabilizing
BA.3 (P62T)	-0.35 kcal/mol	Destabilizing

4-dienamide (Lys125) with binding affinities of -3.9, -3.8 and -2.6 kcal/mol, respectively. The list of the residue interactions and binding affinity for all the 112 compounds is listed in Table A1 (refer Supplementary Data).

Protein-Ligand Binding Analysis
Protein-ligand interaction analysis was done using the PLIP server to check the molecular interactions between Nsp1 N-terminal and the top five compounds. Stigmasterol formed hydrophobic interaction with three residues of Ile95, Gln96 and Arg99 with distances of 3.63, 3.92 and 3.95, respectively (Figure 5) (Table 4).

**Table 3.** List of five compounds that interacted with the target residues

PubChem CID	Compound Names	IUPAC Names	Interacted Target Residues	Binding Affinity (kcal/mol)
5280794	Stigmasterol	(3S,8S,9S,10R,13R,14S,17R)-17-[(E,2R,5S)-5-ethyl-6-methylhept-3-en-2yl]-10,13-dimethyl-2,3,4,7,8,9,11,12,14,15,16,17-dodecahydro-1H-cyclopenta[a]phenanthren-3-ol	Arg99	-4.7
125213	N-feruloyltyramine	3-(4-hydroxy-3-methoxyphenyl)-N-[2-(4hydroxyphenyl) ethyl]prop-2-enamide	Arg99, Arg124, Lys125	-4.4
222284	beta-Sitosterol	(3S,8S,9S,10R,13R,14S,17R)-17-[(2R,5R)-5-ethyl-6-methylheptan-2-yl]-10,13dimethyl-2,3,4,7,8,9,11,12,14,15,16,17dodecahydro-1H-cyclopenta[a]phenanthren3-ol	Arg99	-3.9
179663	13-(1,3-benzodioxol-5-yl)-N-(2methylpropyl) trideca-2,4,12-trienamide	13-(1,3-benzodioxol-5-yl)-N-(2methylpropyl)trideca-2,4,12-trienamide	Glu36	-3.8
56633806	N-(2-methylpropyl) octadeca-2-4dienamide	N-(2-methylpropyl)octadeca-2,4-dienamide	Lys125	-2.6
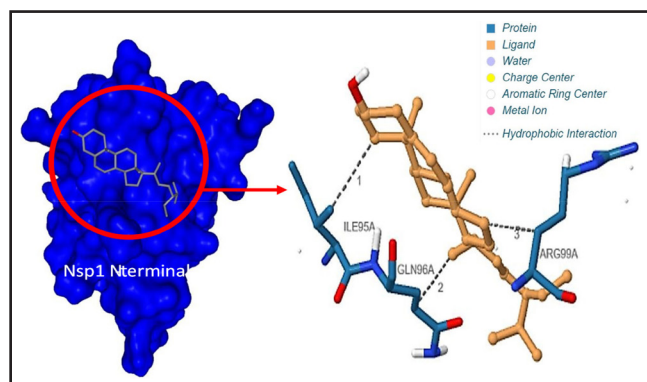
Figure 5. Protein-ligand complex of Nsp1 N-terminal and stigmasterol. Nsp1 N-terminal highlighted in dark blue and stigmasterol highlighted in cyan (left). Hydrophobic interactions highlighted in black dotted lines (right).

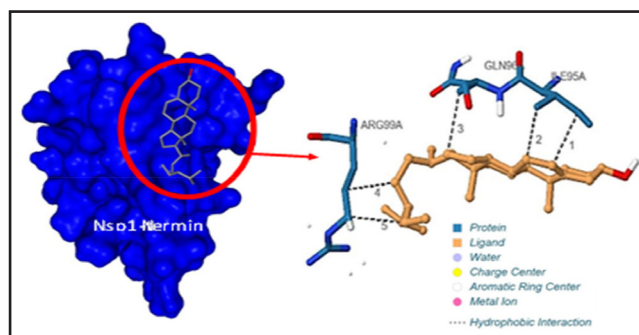**Table 4.** Hydrophobic interaction between Nsp1 and stigmasterol

Index	Residue	Distance (Å)	Types of Interactions
1	Ile95	3.63	Hydrophobic
2	Gln96	3.92	Hydrophobic
3	Arg99	3.95	Hydrophobic
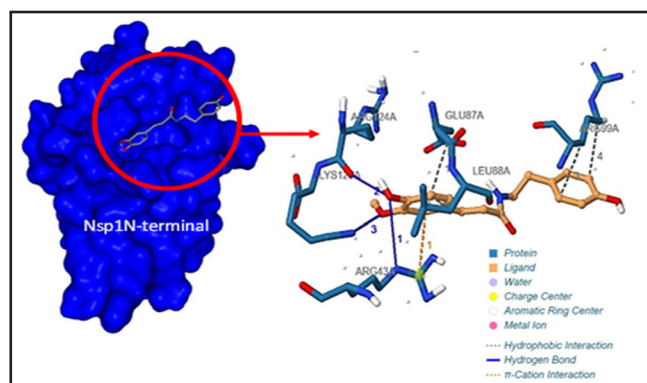
Figure 6. Protein-ligand complex of Nsp1 N-terminal and N-feruloyltyramine. Nsp1 N-terminal is highlighted dark blue and N-feruloyltyramine in cyan (left). Hydrophobic interactions highlighted in black dotted lines, hydrogen bonds are highlighted in blue lines and π-cation interaction is highlighted in orange dotted line (right).

Table 5. Hydrophobic interaction, hydrogen bonds and π-cation between Nsp1 and N-feruloyltyramine

| Index	Residue	Distance between hydrogen and acceptor atoms (Å)	Types of Interactions
1	Glu87	3.68	Hydrophobic
2	Leu88	3.96	Hydrophobic
3	Arg99	3.71	Hydrophobic
4	Arg99	3.70	Hydrophobic
1	Arg43	3.01	Hydrogen Bond
2	Arg124	1.90	Hydrogen Bond
3	Lys125	2.58	Hydrogen Bond
1	Arg43	4.34	π-Cation

Figure 7. Protein-ligand complex of Nsp1 N-terminal and beta-Sitosterol. Nsp1 N-terminal is highlighted in dark blue with beta-sitosterol highlighted in cyan (left). Hydrophobic interactions are highlighted in black dotted lines (right).

Table 6. Hydrophobic interaction between Nsp1 and beta-sitosterol

Index	Residue	Distance (Å)	Types of Interactions
1	Ile95	3.42	Hydrophobic
2	Ile95	3.84	Hydrophobic
3	Gln96	3.44	Hydrophobic
4	Arg99	3.59	Hydrophobic
5	Arg99	3.62	Hydrophobic

Interestingly, besides hydrophobic interaction and hydrogen bonding, π-cation interactions were also observed between N-feruloyltyramine and the protein. Here, the compound formed hydrophobic interactions with Glu87 (3.68), Leu88 (3.96) and Arg99 (3.71 and 3.70). Hydrogen bonds in the protein-ligand complex were found at residues Arg43, Arg124 and Lys124 with the distance between the hydrogen and acceptor atoms of 3.01, 1.90 and 2.58, respectively. As for π-cation, the aromatic ring of N-feruloyltyramine interacted with Arg43 at 4.34 (Figure 6) (Table 5).

Whilst beta-sitosterol formed five hydrophobic interactions with the protein. Two interactions occurred with the same residues which are Ile95 (3.42 and 3.84) and Arg99 (3.59 and 3.62) while the other one with Gln96 (3.44) (Figure 7) (Table 6). Compound 13-(1,3-benzodioxol-5-yl)-N-(2-methylpropyl) trideca-2,4,12trienamide was found to have hydrophobic interactions with the protein at Val35 (3.76), Glu36 (3.57), Leu39 (3.72 and 3.80) and Tyr97 (3.64) (Figure 8) (Table 7).
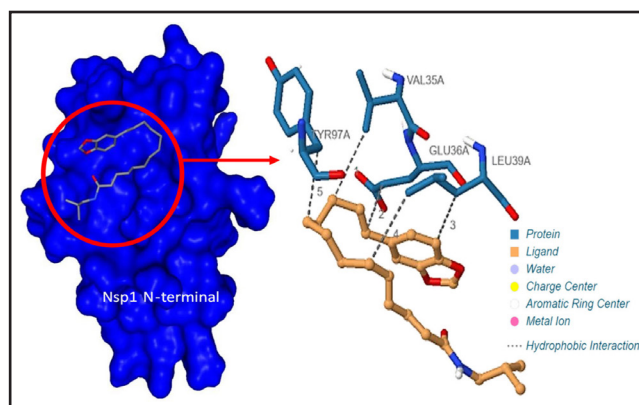
Figure 8. Protein-ligand complex of NSP1 N-terminal and 13-(1,3-benzodioxol-5-yl)-N-(2-methylpropyl) triceda-2,4,12-trienamide. Left: Nsp1 N-terminal (dark blue) with 13-(1,3-benzodioxol-5-yl)-N-(2methylpropyl) trideca-2,4,12-trienamide (cyan). Right: hydrophobic interactions (black dotted lines) of the ligand (ochre) with the residues.
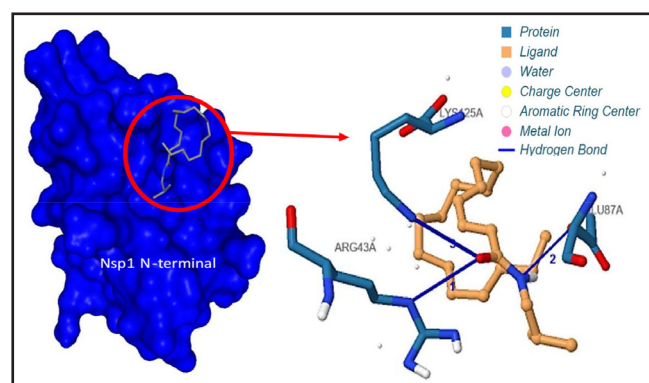
Table 7. Data on the hydrophobic interaction between Nsp1 and 13-(1,3benzodioxol-5-yl)-N-(2-methylpropyl) trideca-2,4,12-trienamide

Index	Residue	Distance (Å)	Types of Interactions
1	Val35	3.76	Hydrophobic
2	Glu36	3.57	Hydrophobic
3	Leu39	3.72	Hydrophobic
4	Leu39	3.80	Hydrophobic
5	Tyr97	3.64	Hydrophobic

Hydrogen bonds were formed between the protein and N-(2-methylpropyl)octadeca2,4-dienamide. And three of the interacted residues were Arg43 (2.75), Glu87 (2.59) and Lys125 (2.97) (Figure 9) (Table 8).

SwissADME Analysis

SwissADME appraises the five potential compounds of *Piper sarmentosum* Roxb. that were successfully formed binding with the target residue(s) of Nsp1. The compounds were checked for their physicochemical properties in six parameters which are lipophilicity, size, polarity, insolubility, in saturation and flexibility. The properties are listed in Table 9. Next, we evaluated the pharmacokinetics of the compounds including GI absorption, BBB permeate, P-gp substrate, inhibitor for five isoenzymes of CYP and skin permeability (Table 10). The drug-likeness analyses were screened in Lipinski, Ghose, Veber, Egan and Muegge filters, alongside the bioavailability score (Table 11).

Molecular Dynamic Simulation

The molecular dynamic simulation was conducted between N-terminal Nsp1 of SARS-CoV-2 (green line) and N-feruloyltyramine (light orange line) complex in CABS-flex 2.0 (Figure 10). The greatest fluctuation was observed at residue number 54 to 70, whereby the line plot of the ligand-Nsp1 complex experienced a greater fluctuation than just the protein itself. In contrast, a significant fluctuation was seen at residue number 74 to 82 in Nsp1 only than the complex.

Figure 9. Protein-ligand complex of Nsp1 N-terminal and N-(2-methylpropyl)octadeca-2,4-dienamide. Left: Nsp1 N-terminal (dark blue) with *N*-(2-methylpropyl)octadeca-2,4dienamide (cyan). Right: hydrogen bonding (blue lines) of the ligand (ochre) with the residues.

Table 8. Data on the hydrogen bonds (blue) between Nsp1 and N-(2methylpropyl)octadeca-2,4-dienamide

Index	Residue	Distance (Å)	Types of Interactions
1	Arg43	2.75	Hydrogen Bond
2	Glu87	2.59	Hydrogen Bond
3	Lys125	2.97	Hydrogen Bond

DISCUSSION

Several studies have reported on mutations that occurred in the N-terminal of Nsp1 of SARS-CoV-2 of Omicron subvariants. Single amino acid substitution was observed in subvariants BA.1 at R99C and, BA.2 and BA.3 shared the same substitution at P62T (Singh *et al.*, 2022; Savellini *et al.*, 2023). Additionally, a five amino acid deletion starting at position 82, was seen in some subvariants of BA.4 (Ak, 2023). However, there are no studies that report on any mutations in N-terminal Nsp1 in BA.5 and BA.6.
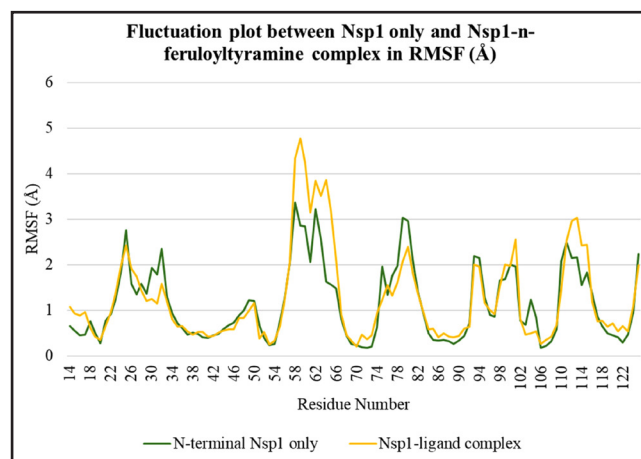
Figure 10. MD simulation of wild-type N-terminal Nsp1 and its ligand-protein complex with N-feruloyltyramine.

Table 9. Physicochemical properties of the potential inhibitors

Compounds	Physicochemical Properties					
	Lipophilicity (XLOGP3)	Size (g/mol)	Polarity (TPSA Å²)	Insolubility Log S (ESOL)	Insaturation (Fraction Csp3)	Flexibility (number of rotatable bonds)
Stigmasterol	8.56	412.69	20.23	-7.46	0.86	5
N-feruloyltyramine	2.10	313.35	78.79	-3.03	0.17	7
beta-Sitosterol	9.34	414.71	20.23	-7.90	0.93	6
13-(1,3-benzodioxol-5-yl)-N-(2methylpropyl) trideca-2,4,12-trienamide	6.81	383.52	47.56	-5.81	0.46	13
N-(2-methylpropyl)octadeca-2,4dienamide	8.73	335.57	29.10	-6.30	0.77	17

Table 10. Pharmacokinetics properties of the potential inhibitors

Compounds	Pharmacokinetics								
	GI absorption	BBB permeate	P-gp substrate	CYP1A2 inhibitor	CYP2C19 inhibitor	CYP2C9 inhibitor	CYP2D6 inhibitor	CYP3A4 inhibitor	Log Kp (skin permeation cm/s)
Stigmasterol	Low	No	No	No	No	Yes	No	No	-2.74
N-feruloyltyramine	High	No	No	No	No	No	Yes	Yes	-6.72
beta-Sitosterol	Low	No	No	No	No	No	No	No	-2.2
13-(1,3-benzodioxol-5yl)-*N*-(2-methylpropyl) trideca-2,4,12-trienamide	High	Yes	No	No	No	Yes	Yes	Yes	-3.8
N-(2-methylpropyl) octadeca-2-4-dienamide	Low	No	No	Yes	No	No	No	No	-2.15

Table 11. Drug-likeness analysis of the potential inhibitors

Compounds	Drug-likeness					
	Lipinski	Ghose	Veber	Egan	Muegge	Bioavailability Score
Stigmasterol	Yes	No	Yes	No	No	0.55
N-feruloyltyramine	Yes	Yes	Yes	Yes	Yes	0.55
beta-Sitosterol	Yes	No	Yes	No	No	0.55
13-(1,3-benzodioxol-5-yl)-N-(2-methylpropyl) trideca-2,4,12-trienamide	Yes	Yes	No	Yes	No	0.55
N-(2-methylpropyl)octadeca-2,4-dienamide	Yes	No	No	No	No	0.55

Comparing the wild-type protein structure of N-terminal Nsp1 of SARS-CoV-2 with each of the Omicron subvariants, BA.1, BA.2, BA.3 and BA.4, there was little difference between them as their RMSD value were less than 2, despite the five amino acids deletion in BA.4 had 0.224 (Abdalla *et al.*, 2022). Thus, it could be argued that these four Omicron subvariants are almost identical to the wild type in terms of protein structure, and possibly retain their function as a stabilizer for the Nsp1 and 40S ribosomal subunit complex. And therefore, redocking the 112 plant compounds of *P. sarmentosum* Roxb. onto the protein structures of N-terminal Nsp1 of BA.1, BA.2, BA.3 and BA.4 was not performed due to their insignificant structural distinction to the wild-type. Though, despite having relatively identical protein structures to the wild type based on the RMSD results, the effect of point mutations could really affect their structural stability and functions (Zeldovich *et al.*, 2007; Vila, 2022). This can be explained based on the DynaMut2 that predicted the N-terminal Nsp1's stability following amino acid substitution based on BA.1, BA.2 and BA.3. The structural prediction for BA.4; nevertheless, was not performed due to the inability of DynaMut2 and the absence of tools or software to carry out analysis on deletion of amino acids. The mutant N-terminal Nsp1 protein of BA.1 was predicted to be more stable than the wild-type due to the mutation at R99C which had positive value for predicted stability change ($\Delta\Delta G^{Stability}$) or Gibbs free energy. This is contrary for BA.2 and BA.3, whereby, the effect of P62T was predicted to destabilize the N-terminal Nsp1 structure due to the negative value of $\Delta\Delta G^{Stability}$. Therefore, the missense mutation in the N-terminal Nsp1 from these three Omicron subvariants could have shifted the overall protein stability in regard to their respective stabilizing or destabilizing effect. The deletion of five amino acids in BA.4 might have greater impact on the protein's overall stability and function.

Sequence with the accession number: YP_009725297 in the NCBI database is a complete amino acid sequence of SARS-CoV-2 Nsp1 (N-terminal) which was sequenced based on the original virus strain, Wuhan-Hu-1 (Wu *et al.*, 2020; Prabhu *et al.*, 2021). This sequence was used for molecular modelling in SWISS-MODEL. This step was indeed crucial since the existing Nsp1 structures in the PDB (PDB ID: 7K3N and 7K7P) were shorter than reported by Clark *et al.* (2021) and Semper *et al.* (2021) which is 127aa. Two of the target residues that are Arg124 and Lys125 were missing in the PDB structures.

Out of the 112 compounds that we screened, only five compounds formed interactions with the target residues. Since N-feruloyltyramine interacted with Arg99, Arg124 and Lys125, it could be a compound with the best potential as an inhibitor for the protein. Stigmasterol and beta-sitosterol formed an interaction with Arg99, in which the inhibitory effect could still be significant but weaker than N-feruloyltyramine. Looking into 13-(1,3-benzodioxol-5-yl)-N-(2-methylpropyl) trideca-2,4,12-trienamide and N(2-methylpropyl) octadeca-2-4-dienamide, that interacted with Glu36 and Lys125, respectively, their inhibitory effect on the Nsp1 N-terminal is very likely to be the weakest. In terms of binding affinity, stigmasterol scored the lowest followed by N-feruloyltyramine, beta-Sitosterol, 13-(1,3-benzodioxol5-yl)-N-(2-methylpropyl) trideca-2,4,12-trienamide and N-(2-methylpropyl) octadeca2-4-dienamide. This indicates that stigmasterol bound strongly to Nsp1 N-terminal whereas N-(2methylpropyl) octadeca-2-4-dienamide has the weakest binding.

PLIP displays the types of molecular interactions that exist in the protein-ligand complex. Hydrophobic interactions are the most common formed by all the potential compounds, except for N-(2methylpropyl) octadeca-2-4-dienamide. The hydrophobic interactions arise from the entropic changes when a carbon atom interacts with a neighbouring atom like carbon or hydrogen only. Hydrophobic interaction is known as the most common type of interaction in protein-ligand complex (de Freitas & Schapira, 2017).

This ubiquitous interaction also drives ligand to be more efficient in binding to the proteins and become the main element in drug-receptor interactions (de Freitas & Schapira, 2017). Another type of molecular interaction that was detected by PLIP between the N-terminal of Nsp1 and N-feruloyltyramine or N-(2-methylpropyl) octadeca-2-4-dienamide is hydrogen bonding. Technically, hydrogen bond in a protein-ligand complex is an intermolecular electrostatic force of attraction between a hydrogen atom and its adjacent atoms which are more electronegative like oxygen and nitrogen (de Freitas & Schapira, 2017). The hydrogen bonding that was reported in PLIP is based on the distance () between hydrogen and the acceptor atoms. Hydrogen bond in drug design are utilized to achieve interaction specificity as they induce stringent distance and geometric constraints and stabilization in the binding of ligands onto protein (de Freitas & Schapira, 2017). The third and unique molecular interaction was found in the protein-ligand complex of Nsp1 N-terminal and N-feruloyltyramine is the π-cation interaction. A π-cation interaction exists when there is an electrostatic pairing occurs between a positively charged atom and an aromatic ring, whereby, the distances between the charge and aromatic ring centre must be less than 6.0 (de Freitas & Schapira, 2017). Although this type of molecular interaction is apparently least observed and used in ligand designs, it is still commonly found in proteins as it provides their functions, structure and stability (de Freitas & Schapira, 2017).

The physicochemical analysis using SwissADME on the five potential compounds of *Piper sarmentosum* Roxb. indicated that N-feruloyltyramine is the most orally bioavailable compound because it falls within the ideal range of the six parameters in the Bioavailability Radar. N-feruloyltyramine has suitable molecular weight, good solubility and not too lipophilic, flexible and polar, except for insaturation (<0.25). On the contrary, the other four potential compounds do not fulfil more than one physicochemical parameter, which makes them very unlikely to be orally bioavailable. Stigmasterol and beta sitosterol are lipophilic and poorly soluble. Meanwhile, 13-(1,3-benzodioxol-5-yl)-N(2-methylpropyl) trideca-2,4,12-trienamide and N-(2-methylpropyl) octadeca-2-4dienamide are too flexible and either moderately or poorly insoluble. However, even a compound is said to be orally bioavailable when it obeys all the six physicochemical parameters' ideal range, its pharmacokinetics and drug-likeness properties should be considered as well (Daina *et al.*, 2017).

SwissADME pharmacokinetics analysis displayed a mixture of outputs on the five potential compounds. Based on GI absorption, BBB permeation, the substrate of P-gp, inhibitors of CYP isoenzymes and the degree of skin permeability, 13-(1,3benzodioxol-5-yl)-N-(2-methylpropyl) trideca-2,4,12-trienamide seems to have the best pharmacokinetics properties among the five compounds due to its high GI absorption and its ability to pass through the blood-brain barrier with moderately impermeable to skin. But it inhibits three isoenzymes of CYP. While N-feruloyltyramine has a high GI absorption, it is very impermeable to skin with the smallest value of log K_p and only inhibits two CYP isoenzymes. However, it is not a BBB permeate which is a minor hindrance to be considered as an orally bioavailable drug candidate. Three other compounds that are stigmasterol, beta-sitosterol and N-(2-methylpropyl) octadeca-2-4dienamide have low GI absorption, unable to permeate through the BBB and have relatively low skin permeability. However, the three compounds are better as CYP isoenzymes-friendly since they either only inhibit one or none of the isoenzymes.

Drug-likeness analysis shows all five compounds are expected to retain 55% bioavailability of their original dosage upon reaching the target site when administered orally. The five drug-likeness filters of Lipinski, Ghose, Veber, Egan and Muegge showed that only N-feruloyltyramine passed all the filters thus indicating that it has good druglike properties. On the other hand, 13-(1,3benzodioxol-5-yl)-N-(2-methylpropyl) trideca-2,4,12-trienamide, stigmasterol and beta-Sitosterol, and N-(2-methylpropyl) octadeca-2-4-dienamide

are implied to have slight, moderately poor and poor drug-likeness, respectively.

However, it is noteworthy to highlight that mutation at the target residues which has been reported before may had a negative impact on the protein functions. Residue mutations can either positively or negatively affect the protein in many aspects including intermolecular interaction, catalytic activity and stability (Studer *et al.*, 2013). Mendez *et al.* (2020) discovered that point mutations at Glu36/Glu37, Arg99 and Arg124/Lys125 in the N-terminal of Nsp1 had caused adverse effects on the viral protein itself. Previous studies also suggested that mutation on certain residues in Nsp1 of SARS-CoV-2 could cause destabilization in its structure and might eventually impede its inhibition efficiency (Hossain *et al.*, 2021; Mou *et al.*, 2021). Ligand binding, too, can induce a conformational change in protein structures, and this in return strongly impacts the protein's binding affinity (Mobley & Dill, 2009).

The MD simulation employed by CABS-flex 2.0 on the wild-type N-terminal Nsp1 and its complex with N-feruloyltyramine showed fluctuation of every protein residue in the structure based on root mean square fluctuation (RMSF) values. The RMSF is a useful indicator that measures the flexibility and fluctuation of each amino acid move over a MD simulation period (Abdalla *et al.*, 2022). The presence of peaks in Figure 2 are due to the loop structures in the protein, where amino acids in these areas experience greater flexibility and fluctuations. Amino acids that make up the α-helix and β-pleated structures, on the other hand, are more rigid than the loop structures, so they are less flexible and have little fluctuations. The interaction between N-terminal Nsp1 and N-feruloyltyramine resulted in many changes to the flexibility of the amino acids, particularly those that fall in the loop regions. The most significant fluctuation can be seen between protein residues 54 to 70, whereby residue number 59 fluctuated from 2.86 (protein only) to the highest value of 4.78 (ligand-protein complex). Overall, the impact of N-feruloyltyramine on the N-terminal Nsp1 has caused significant changes to the RMSF of protein residues in the loop region as they underwent greater flexibility and fluctuations than protein itself. And these could negatively impact the protein's stability and function. This is because there is a correlation between RMSF and the function of proteins (Berhanu & Masunov, 2011; Bavi *et al.*, 2016).

CONCLUSION

The most promising inhibitor of *P. sarmentosum* Roxb., N-feruloyltyramine, had a significant effect on the N-terminal Nsp1 of SARS-CoV-2 by increasing its flexibility around the loop regions of the protein. This in turn could disrupt the protein's stability, which later impedes its function to strengthen the interaction between Nsp1 and the host's 40S ribosomal subunit complex. Although the N-terminal Nsp1 protein of the Omicron subvariants: BA.1, BA.2, BA.3 and BA.4, are nearly identical to the wild-type in the aspect of structure; their stability and even function are affected due to the missense mutation and amino acids deletion.

Conflict of Interest
The author declares that they have no conflict of interests.

REFERENCES

Abdalla, M., Eltayb, W.A., El-Arabey, A.A., Singh, K. & Jiang, X. (2022). Molecular dynamic study of SARS-CoV-2 with various S protein mutations and their effect on thermodynamic properties. *Computers in Biology and Medicine* **141**: 105025.
https://doi.org/10.1016/J.COMPBIOMED.2021.105025

Adasme, M.F., Linnemann, K.L., Bolz, S.N., Kaiser, F., Salentin, S., Haupt, V.J. & Schroeder, M. (2021). PLIP 2021: expanding the scope of the protein–ligand interaction profiler to DNA and RNA. *Nucleic Acids Research* **49**: W530-W534. https://doi.org/10.1093/nar/gkab294

Adejoro, I.A., Babatunde, D.D. & Tolufashe, G.F. (2020). Molecular docking and dynamic simulations of some medicinal plants compounds against SARS-CoV-2: an *in silico* study. *Journal of Taibah University for Science* **14**: 1563-1570. https://doi.org/10.1080/16583655.2020.1848049

Ak, C. (2023). The [82]GHVMV and [141]KSF deletions in the Nsp1 protein of ORF1ab polyprotein favour the creation of immune-weak SARS-CoV-2. *SunText Review of Virology* **3**: 137. https://doi.org/10.51737/2766-5003.2023.037

Almeida, M.S., Johnson, M.A., Herrmann, T., Geralt, M. & Wuthrich, K. (2007). Novel β-barrel fold in the nuclear magnetic resonance structure of the replicase nonstructural protein 1 from the severe acute respiratory syndrome coronavirus. *Journal of Virology* **81**: 3151-3161. https://doi.org/10.1128/jvi.01939-06

Arya, R., Kumari, S., Pandey, B., Mistry, H., Bihani, S.C., Das, A., Prashar, V., Gupta, G.D., Panicker, L. & Kumar, M. (2021). Structural insights into SARS-CoV-2 proteins. *Journal of Molecular Biology* **433**: 166725. https://doi.org/10.1016/j.jmb.2020.11.024

Banerjee, A.K., Blanco, M.R., Bruce, E.A., Honson, D.D., Chen, L.M., Chow, A., Bhat, P., Ollikainen, N., Quinodoz, S.A., Loney, C. *et al.* (2020). SARS-CoV-2 disrupts splicing, translation, and protein trafficking to suppress host defenses. *Cell* **183**: 1325-1339. https://doi.org/10.1016/j.cell.2020.10.004

Bavi, R., Kumar, R., Choi, L. & Lee, K.W. (2016). Exploration of novel inhibitors for Bruton's tyrosine kinase by 3D QSAR modeling and molecular dynamics simulation. *PLOS ONE* **11**: e0147190. https://doi.org/10.1371/JOURNAL.PONE.0147190

Berhanu, W.M. & Masunov, A.E. (2011). Molecular dynamic simulation of wild type and mutants of the polymorphic amyloid NNQNTF segments of elk prion: structural stability and thermodynamic of association. *Biopolymers* **95**: 573-590. https://doi.org/10.1002/BIP.21611

Clark, L.K., Green, T.J. & Petit, C.M. (2021). Structure of nonstructural protein 1 from SARS-CoV-2. *Journal of Virology* **95**: e02019-20. https://doi.org/10.1128/jvi.02019-20

Corpet, F. (1988). Multiple sequence alignment with hierarchical clustering. *Nucleic Acids Research* **16**: 10881-10890. https://doi.org/10.1093/NAR/16.22.10881

Daina, A., Michielin, O. & Zoete, V. (2017). SwissADME: a free web tool to evaluate pharmacokinetics, drug-likeness and medicinal chemistry friendliness of small molecules. *Scientific Reports* **7**: 42717. https://doi.org/10.1038/srep42717

Eberhardt, J., Santos-Martins, D., Tillack, A.F. & Forli, S. (2021). AutoDock Vina 1.2.0: new docking methods, expanded force field, and python bindings. *Journal of chemical information and modeling* **61**: 3891-3898. https://doi.org/10.1021/acs.jcim.1c00203

Fährrolfes, R., Bietz, S., Flachsenberg, F., Meyder, A., Nittinger, E., Otto, T., Volkamer, A. & Rarey, M. (2017). Proteins*Plus*: a web portal for structure analysis of macromolecules. *Nucleic Acids Research* **45**: W337-W343. https://doi.org/10.1093/nar/gkx333

de Freitas, R.F. & Schapira, M. (2017). A systematic analysis of atomic protein-ligand interactions in the PDB. *MedChemComm* **8**: 1970-1981. https://doi.org/10.1039/C7MD00381A

Gorkhali, R., Koirala, P., Rijal, S., Mainali, A., Baral, A. & Bhattarai, H.K. (2021). Structure and function of major SARS-CoV-2 and SARS-CoV proteins. *Bioinformatics and Biology Insights* **15**: 11779322211025876. https://doi.org/10.1177/11779322211025876

Graziadei, A., Schildhauer, F., Spahn, C., Kraushar, M. & Rappsilber, J. (2022). SARS-CoV-2 Nsp1 N-terminal and linker regions as a platform for host translational shutoff. *BioRxiv 2022-02* [**Preprint**]. https://doi.org/10.1101/2022.02.10.479924

Hamidi, J.A., Ismaili, N.H., Ahmadi, F.B. & Lajisi, N.H. (1996). Antiviral and cytotoxic activities of some plants used in Malaysian indigenous medicine. *Pertanika Joural of Tropical Agricultural Science* **19**: 129-136.

Hamidi, J. A., Ismaili, N. H., Ahmadi, F. B., & Lajisi, N. H. (1996). Antiviral and cytotoxic activities of some plants used in Malaysian indigenous medicine. *Pertanika J. Trop. Agric. Sci, 19*: 129-136.

Hossain, M.U., Bhattacharjee, A., Emon, M.T.H., Chowdhury, Z.M., Ahammad, I., Mosaib, M.G., Moniruzzaman, M., Rahman, M.H., Islam, M.N., Ahmed, I. *et al.* (2021). Novel mutations in NSP-1 and PLPro of SARS-CoV-2 NIB-1 genome mount for effective therapeutics. *Journal of Genetic Engineering and Biotechnology* **19**: 52. https://doi.org/10.1186/s43141-021-00152-z

Kamitani, W., Huang, C., Narayanan, K., Lokugamage, K.G. & Makino, S. (2009). A two-pronged strategy to suppress host protein synthesis by SARS coronavirus Nsp1 protein. *Nature Structural & Molecular Biology* **16**: 1134-1140. https://doi.org/10.1038/nsmb.1680

Kumar, A., Kumar, A., Kumar, P., Garg, N. & Giri, R. (2021). SARS-CoV-2 NSP1 C-terminal (residues 131-180) is an intrinsically disordered region in isolation. *Current Research in Virological Science* **2**: 100007. https://doi.org/10.1016/j.crviro.2021.100007

Kuriata, A., Gierut, A.M., Oleniecki, T., Ciemny, M.P., Kolinski, A., Kurcinski, M. & Kmiecik, S. (2018). CABS-flex 2.0: a web server for fast simulations of flexibility of protein structures. *Nucleic Acids Research* **46**: W338-W343. https://doi.org/10.1093/NAR/GKY356

Mendez, A.S., Ly, M., González-Sánchez, A.M., Hartenian, E., Ingolia, N.T., Cate, J.H. & Glaunsinger, B.A. (2021). The N-terminal domain of SARS-CoV-2 nsp1 plays key roles in suppression of cellular gene expression and preservation of viral gene expression. *Cell Reports* **37**: 109841. https://doi.org/10.1016/j.celrep.2021.109841

Mobley, D.L. & Dill, K.A. (2009). Binding of small-molecule ligands to proteins:"what you see" is not always "what you get". *Structure* **17**: 489-498. https://doi.org/10.1016/j.str.2009.02.010

Mou, K., Mukhtar, F., Khan, M.T., Darwish, D.B., Peng, S., Muhammad, S., Al-Sehemi, A.G. & Wei, D.Q. (2021). Emerging mutations in Nsp1 of SARS-CoV-2 and their effect on the structural stability. *Pathogens* **10**: 1285. https://doi.org/10.3390/pathogens10101285

Narayanan, K., Huang, C., Lokugamage, K., Kamitani, W., Ikegami, T., Tseng, C.T.K. & Makino, S. (2008). Severe acute respiratory syndrome coronavirus nsp1 suppresses host gene expression, including that of type I interferon, in infected cells. *Journal of Virology* **82**: 4471-4479. https://doi.org/10.1128/jvi.02472-07

O'Boyle, N.M., Banck, M., James, C.A., Morley, C., Vandermeersch, T. & Hutchison, G.R. (2011). Open Babel: an open chemical toolbox. *Journal of Cheminformatics* **3**: 33. https://doi.org/10.1186/1758-2946-3-33

Prabhu, D., Rajamanikandan, S., Sureshan, M., Jeyakanthan, J. & Saraboji, K. (2021). Modelling studies reveal the importance of the C-terminal inter motif loop of NSP1 as a promising target site for drug discovery and screening of potential phytochemicals to combat SARS-CoV-2. *Journal of Molecular Graphics and Modelling* **106**: 107920. https://doi.org/10.1016/j.jmgm.2021.107920

Rodrigues, C.H.M., Pires, D.E.V. & Ascher, D.B. (2021). DynaMut2: assessing changes in stability and flexibility upon single and multiple point missense mutations. *Protein Science* **30**: 60-69. https://doi.org/10.1002/PRO.3942

Rukachaisirikul, T., Siriwattanakit, P., Sukcharoenphol, K., Wongvein, C., Ruttanaweang, P., Wongwattanavuch, P. & Suksamrarn, A. (2004). Chemical constituents and bioactivity of *Piper sarmentosum*. *Journal of Ethnopharmacology* **93**: 173-176. https://doi.org/10.1016/j.jep.2004.01.022

Savellini, G.G., Anichini, G. & Cusi, M.G. (2023). SARS-CoV-2 omicron sub-lineages differentially modulate interferon response in human lung epithelial cells. *Virus Research* **332**: 199134. https://doi.org/10.1016/j.virusres.2023.199134

Samy, J., Sugumaran, M. & Lee, K.L. (2014). 100 useful herbs of Malaysia and Singapore: an introduction to their medicinal, culinary, aromatic and cosmetic uses. Wong, K.M. (editor). Singapore: Marshall Cavendish.

Sanner, M.F. (1999). Python: a programming language for software integration and development. *Journal of Molecular Graphics and Modelling* **17**: 57-61.

Schöning-Stierand, K., Diedrich, K., Fährrolfes, R., Flachsenberg, F., Meyder, A., Nittinger, E., Steinegger, R. & Rarey, M. (2020). Proteins*Plus*: Interactive analysis of protein-ligand binding interfaces. *Nucleic Acids Research* **48**: W48-W53. https://doi.org/10.1093/nar/gkaa235

Schubert, K., Karousis, E.D., Jomaa, A., Scaiola, A., Echeverria, B., Gurzeler, L.A., Leibundgur, M., Theil, V. & Ban, N. (2020). SARS-CoV-2 Nsp1 binds the ribosomal mRNA channel to inhibit translation. *Nature Structural & Molecular Biology* **27**: 959-966. https://doi.org/10.1038/s41594-020-0511-8

Semper, C., Watanabe, N. & Savchenko, A. (2021). Structural characterization of nonstructural protein 1 from SARS-CoV-2. *IScience* **24**: 101903. https://doi.org/10.1016/j.isci.2020.101903

Shi, M., Wang, L., Fontana, P., Vora, S., Zhang, Y., Fu, T.M., Lieberman, J. & Wu, H. (2020). SARS-CoV-2 Nsp1 suppresses host but not viral translation through a bipartite mechanism. *BioRxiv 302901* [**Preprint**]. https://doi.org/10.1101/2020.09.18.302901

Singh, P., Negi, S.S., Bhargava, A., Kolla, V.P. & Arora, R.D. (2022). A preliminary genomic analysis of the Omicron variants of SARS-CoV-2 in Central India during the third wave of the COVID-19 pandemic. *Archives of Medical Research* **53**: 574-584. https://doi.org/10.1016/j.arcmed.2022.08.006

Singh, R., Bhardwaj, V.K., Das, P. & Purohit, R. (2021). A computational approach for rational discovery of inhibitors for non-structural protein 1 of SARS-CoV-2. *Computers in Biology and Medicine* **135**: 104555. https://doi.org/10.1016/j.compbiomed.2021.104555

Studer, R.A., Dessailly, B.H. & Orengo, C.A. (2013). Residue mutations and their impact on protein structure and function: detecting beneficial and pathogenic changes. *Biochemical Journal* **449**: 581-594. https://doi.org/10.1042/BJ20121221

Sun, X., Chen, W., Dai, W., Xin, H., Rahmand, K., Wang, Y., Zhang, J., Zhang, S., Xu, L. & Han, T. (2020). *Piper sarmentosum* Roxb.: A review on its botany, traditional uses, phytochemistry, and pharmacological activities. *Journal of Ethnopharmacology* **263**: 112897. https://doi.org/10.1016/j.jep.2020.112897

Thoms, M., Buschauer, R., Ameismeier, M., Koepke, L., Denk, T., Hirschenberger, M., Kratzat, H., Hayn, M., Mackens-Kiani, T., Cheng, J. *et al*. (2020). Structural basis for translational shutdown and immune evasion by the Nsp1 protein of SARS-CoV-2. *Science* **369**: 1249-1255. https://doi.org/10.1126/science.abc8665

Trott, O. & Olson, A.J. (2010). AutoDock Vina: improving the speed and accuracy of docking with a new scoring function, efficient optimization, and multithreading. *Journal of Computational Chemistry* **31**: 455-461. https://doi.org/10.1002/jcc.21334

Vila, J.A. (2022). Proteins' evolution upon point mutations. *ACS Omega* **7**: 14371-14376. https://doi.org/10.1021/acsomega.2c01407

Wu, F., Zhao, S., Yu, B., Chen, Y.M., Wang, W., Song, Z.G., Hu, Y., Tao, Z.W., Tin, J.H., Pei, Y.Y. *et al*. (2020). A new coronavirus associated with human respiratory disease in China. *Nature* **579**: 265-269. https://doi.org/10.1038/s41586-020-2008-3

Yuan, S., Balaji, S., Lomakin, I.B. & Xiong, Y. (2021). Coronavirus Nsp1: immune response suppression and protein expression inhibition. *Frontiers in Microbiology* **12**: 752214. https://doi.org/10.3389/fmicb.2021.752214

Yuan, S., Peng, L., Park, J.J., Hu, Y., Devarkar, S.C., Dong, M.B., Shen, Q., Wu, S., Chen, S. *et al*. (2020). Nonstructural protein 1 of SARS-CoV-2 is a potent pathogenicity factor redirecting host protein synthesis machinery toward viral RNA. *Molecular Cell* **80**: 1055-1066. https://doi.org/10.1016/j.molcel.2020.10.034

Zaidan, M.R., Noor Rain, A., Badrul, A.R., Adlin, A., Norazah, A. & Zakiah, I. (2005). *In vitro* screening of five local medicinal plants for antibacterial activity using disc diffusion method. *Tropical Biomedicine* **22**: 165-170.

Zeldovich, K.B., Chen, P. & Shakhnovich, E.I. (2007). Protein stability imposes limits on organism complexity and speed of molecular evolution. *Proceedings of the National Academy of Sciences* **104**: 16152-16157. https://doi.org/10.1073/pnas.0705366104